Polarization-independent electronically tunable liquid-crystal spectacles

Yi-Hsin Lin,[1,*] Hao-Hsin Huang,[1] Wei-Cheng Cheng,[1] Victor Reshetnyak,[2,3] Ting-Wei Huang,[1] Chang-Chiang Cheng,[4] Mei-Wen Jao,[4] Chih-Lung Lin,[4] Yu-Shih Tsou,[4] Yung-Hsun Wu,[4] and Chiu-Lien Yang[4]

[1] *Department of Photonics, College of Electrical and Computer Engineering, National Yang Ming Chiao Tung University, Hsinchu, Taiwan*

[2] *Theoretical Physics Department, Taras Shevchenko National University of Kyiv, Kyiv, 01601, Ukraine*

[3] *School of Physics and Astronomy, University of Leeds, Leeds, LS2 9JT, United Kingdom*

[4] *Technology Development Center, Innolux Corporation, Miaoli, Taiwan*

(Received 14 June 2024; revised 20 May 2025; accepted 11 July 2025; published 29 August 2025)

Since Benjamin Franklin proposed the first bifocal lenses in 1784 and Bernard Maitenaz invented the first varifocal lenses in 1959, researchers worldwide have been actively working on developing electronically switchable lenses for spectacles with the goal of addressing vision issues faced by individuals with both presbyopia and myopia. Liquid-crystal (LC) refractive or diffractive Fresnel lenses have emerged as a promising solution. However, the degradation of incoherent imaging, caused by microstructures, diffraction, and chromatic aberration, makes LC refractive or diffractive Fresnel lenses not suitable for spectacle applications. LC gradient index (GRIN) lenses have been suggested and successfully demonstrated in laboratories as an alternative to LC Fresnel lenses. However, how to bridge the gaps between engineering and physics as well as from laboratory to industry is still a question. To address these gaps, we present here electrically switchable spectacles based on LC GRIN lenses, which have the potential for mass production. Additionally, we discuss the optical principles underlying polarization-independent LC GRIN lenses, based on a wave-plate model. We present a breakthrough that is a significant advancement in LC-based tunable spectacles and that may provide vision correction for individuals worldwide. The impacts of this study are not only ophthalmic applications but also machine vision for artificial intelligence as well as augmented reality.

DOI: 10.1103/3m2d-k24l

I. INTRODUCTION

One thousand years ago, the Arab scholar and astronomer Ibn al-Heitam was the first to suggest using lenses to improve people's vision [1,2]. Italian monks realized the lens idea by smoothing "reading stone" made of rock crystal and quartz to help people who suffered from presbyopia, and their approach was used until the 13th century [2]. It was not understood how lenses correct presbyopia and myopia until the explanation was given by Johannes Kepler in 1604 [3]. Bifocals lenses, invented by Benjamin Franklin in 1784, solved the vision problem for people who suffered from both presbyopia and myopia by providing concave and convex lenses at different locations of a prescription lens [4]. The discomfort and dizziness associated with bifocal lenses inspired Maitenaz [5] to invent progressive lenses in 1959. Progressive lenses possess a gradient distribution of focal lengths from negative to positive focal lengths. Around 1970, progressive lenses were successfully manufactured in France and the USA [6]. However, unwanted astigmatism and an uncomfortable eye-training process, when people had to move their eyes to see different zones of the lens for distant or near objects, inspired scientists to explore switchable electronic lenses [6]. In 1979, Sato [7] proposed the first electrically tunable liquid-crystal (LC) lenses by filling a cavity between two curved glasses with nematic liquid crystals. The light speed of incident linearly polarized light changes because the refractive index of LCs in the planoconcave or planoconvex cavity changes with temperature or applied electric fields. This is similar to what happens with a lens with an inhomogeneous refractive index, so the collimated light focuses to different locations under external stimuli. In 1985, Sato *et al.* [8] proposed a tunable polarizer-free liquid-crystal Fresnel lens by stacking two LC refractive Fresnel lenses with mutually orthogonal optical axes, although they did not fully explain the concept of polarizer-free LC optics. Many years later, in 2006, Li *et al.* [9] demonstrated switchable diffractive Fresnel lenses for ophthalmic applications

*Contact author: yilin@nycu.edu.tw

without a polarizer by means of a double-layered structure similar to that proposed by Sato *et al.* However, diffractive lenses suffer from transverse chromatic aberration and inflexibility in adjustment of astigmatism, and most importantly, diffraction always degrades image quality, especially for incoherent imaging [6,10–13]. In 2004, Douali and Silver [14] designed self-adjustable eyeglasses with a fluid reservoir enclosed by a flexible membrane. The focal length of the lenses is changed by the pumping in and out of fluid to change the curvature of the lenses. The curvature of the lens can be also adjusted by use of the electrowetting effect [15]. However, the unwanted effect of gravity, unwanted interface reflection, the bulky system, and inflexibility to adjust the aberration and astigmatism tailored to the eyes result in limitation in ophthalmic applications [16]. Alvarez lenses, proposed by Nobel laureate Alvarez, change focal lengths by laterally translating the position of two closely spaced lenses [17,18]. However, Alvarez lenses as well as liquid lenses are difficult to incorporate into standard eyeglass frames [6]. The increasing longevity of humans inevitably drives the pursuit of better solutions for prescription lenses to address both myopia, which is becoming more common among young people, and presbyopia, which is an unavoidable consequence of the aging of the eye's crystalline lens. Instead of Fresnel lenses, LC gradient index (GRIN) lenses based on slit-patterned or hole-patterned electrodes were proposed in 1984 and 1989 [19,20]. LC GRIN lenses offer spatially tunable refractive indices as LC orientations vary in response to an inhomogeneous electric field (usually generated by a hole-patterned electrode) [10,11,21–24]. How to exploit LC GRIN lens in ophthalmic applications was well explained in 2013 [21]. Without pixelated electrodes, numerous diffractive Fresnel ring electrodes, and nonplanar refractive Fresnel lenses, LC GRIN lenses provide a promising imaging solution for incoherent imaging as switchable prescription lenses. However, because of the so-called power law and the intrinsic limitation of nematic LCs in chemistry and in physics, LC GRIN lenses have been overlooked in prescription lenses for a long time [10,11,21–24]. In 2023, we proposed how to overcome the power law to increase the aperture size and also demonstrated electrically tunable progressive lenses [24]. Nevertheless, to date, studies of LC GRIN lenses are in the proof-of-concept stage. How to manufacture LC GRIN lenses for practical mass production is still a question. Moreover, the general principle of polarizer-free LC GRIN lenses is still not clear even though some studies tried to explain it in an incomplete way [8–10,21,22,25–30]. In this paper, we discuss how to manufacture polarizer-free electrically switchable spectacles using nematic liquid crystals and bridge academic varifocal LC lenses from laboratory to industrial mass production. The general optical principle of polarization-independent LC GRIN lenses is explained comprehensively on the basis of the wave-plate model. The suggested structure is based on two layered LC GRIN lenses with mutually orthogonal alignment. The fabrication process and the electronics in eyeglass frames are introduced. We show that polarization-independent, electrically switchable spectacles based on LC GRIN lenses might be suitable for mass production. We believe this report provides a solution for prescription lenses, which may benefit humans in a revolutionary way.

II. PRELIMINARY ESTIMATES FOR POLARIZATION-INDEPENDENT LC GRIN LENSES

Nematic LC molecules, with a rodlike chemical structure, act as a uniaxial medium when the molecules are aligned well in proper ways [31,32]. We explain the general principles of polarization-independent LC phase modulations on the basis of the wave-plate model in crystal optics and then extend the principles to a LC GRIN lens. Assume that the incident wave $|\vec{\Psi}_{\text{in}}(z,t)\rangle$ is an unpolarized plane wave propagating along the z direction, which means the light beam is randomly polarized or, in other words, is composed of a rapidly-time-varying succession of different polarizations [31]. According to this definition, $|\vec{\Psi}_{\text{in}}(z,t)\rangle$ is expressed as

$$|\vec{\Psi}_{\text{in}}\rangle = e^{-j(k_0 z-\omega t)}(\alpha|x\rangle + \beta|y\rangle), \tag{1}$$

where α and β are time-varying complex numbers, $|x\rangle$ and $|y\rangle$ are x-linearly-polarized and y-linearly-polarized light, k_0 is the wave number in free space, ω is the angular frequency of light, and t is time. When light propagates in a uniaxial wave plate or a LC wave plate with the corresponding transmittance operator H_{LC}, the outgoing wave $|\vec{\Psi}_{\text{out}}\rangle$ is given by

$$|\vec{\Psi}_{\text{out}}\rangle = H_{\text{LC}}|\vec{\Psi}_{\text{in}}\rangle. \tag{2}$$

Since nematic LCs are uniaxial optically anisotropic liquids, their extraordinary refractive index depends on the angle $\tilde{\theta}$ between the optical axis (director) and the linear polarization of light (extraordinary wave). Because of the nematic LC director anchoring at the cell substrates and the applied voltage V, the angle $\tilde{\theta}$ generally depends on the spatial coordinates and applied voltage $\tilde{\theta}(r,V)$, and therefore the extraordinary refractive index also becomes spatially inhomogeneous:

$$\tilde{n}_{\text{eff}}(r,V) = \frac{n_e n_o}{[n_e^2 \sin^2\tilde{\theta}(r,V) + n_o^2 \cos^2\tilde{\theta}(r,V)]^{1/2}}, \tag{3}$$

where n_e and n_o are the extraordinary refractive index and the ordinary refractive index. The corresponding phase

retardation for the extraordinary polarized light propagating in the z direction is given by

$$\phi_e(r) = k_0 \int_0^d \tilde{n}_{\text{eff}}(r, z, V)\mathrm{d}z, \tag{4}$$

where d is the thickness. Equation (4) is valid only when the polar angle of the LC director changes only with z, and not with its azimuthal angle. For simplicity, it is convenient to introduce $n_{\text{eff}}(r, V)$, the effective refractive index averaged over the LC slab thickness,

$$n_{\text{eff}}(r, V) = \frac{1}{d}\int_0^d \tilde{n}_{\text{eff}}(r, z, V)\mathrm{d}z, \tag{5}$$

and the corresponding averaged angle of the nematic optical axis $\theta'(r, V)$ found from

$$n_{\text{eff}}(r, V) = \frac{n_e n_o}{[n_e^2 \sin^2\theta'(r, V) + n_o^2 \cos^2\theta'(r, V)]^{1/2}}. \tag{6}$$

In what follows, we call the direction given by $\theta'(r, V)$ the "slow axis." Assume that the fast and slow axes of the LC wave plate are parallel to the x axis and the y axis, respectively. That implies that x-linearly-polarized light and y-linearly-polarized light correspond to two eigenpolarizations of a LC wave plate: ordinary wave and extraordinary wave, respectively. When x-and-y-linearly polarized light travels through the LC wave plate, the polarizations do not change, but the phases accumulate: ϕ_o and ϕ_e for x-linearly polarized light and y-linearly polarized light, respectively. As a result, H_{LC} operation onto two eigenpolarizations is expressed as

$$H_{\text{LC},f\,\|x}|x\rangle = e^{j\phi_o}|x\rangle, \tag{7}$$

$$H_{\text{LC},f\,\|x}|y\rangle = e^{j\phi_e}|y\rangle, \tag{8}$$

where $\phi_o = k_0 n_o d$ and $\phi_e = k_0 n_{\text{eff}}(\theta')d$. From the above, Eq. (2) becomes

$$|\vec{\Psi}_{\text{out}}\rangle = H_{\text{LC}}|\vec{\Psi}_{\text{in}}\rangle = \begin{bmatrix} e^{j\phi_o} & 0 \\ 0 & e^{j\phi_e} \end{bmatrix} |\vec{\Psi}_{\text{in}}\rangle. \tag{9}$$

Assume that light propagates through N uniaxial wave plates and the fast axis of the Nth wave plate is θ_N with respect to the x axis of the laboratory coordinate, as depicted in Fig. 1. The operator of the Nth LC wave plate $H_{\text{LC},N}$ is then modified as [32]

$$H_{\text{LC},N} = R(-\theta_N)e^{j\tilde{\phi}_N}\begin{bmatrix} e^{-j(\Gamma_N/2)} & 0 \\ 0 & e^{j(\Gamma_N/2)} \end{bmatrix} R(\theta_N), \tag{10}$$

where $R(\theta_N)$ is the rotational matrix:

$$R(\theta_N) = \begin{bmatrix} \cos(\theta_N) & \sin(\theta_N) \\ -\sin(\theta_N) & \cos(\theta_N) \end{bmatrix}. \tag{11}$$

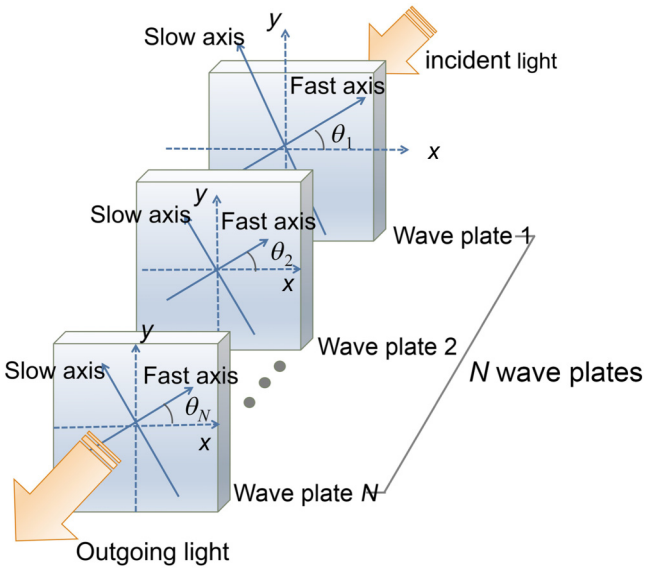

FIG. 1. General principle of polarizer-free LC electronic lenses with N uniaxial wave plates.

In Eq. (10), Γ_N is the phase retardation, $\Gamma_N = k_0(n_{e,N} - n_{o,N})d_N$, and $\tilde{\phi}_N$ is the optical phase, $\tilde{\phi}_N = (k_0/2)(n_{e,N} + n_{o,N})d_{\text{N}}$, where d_N is the thickness of the Nth LC wave plate.

Then we express the outgoing light $|\vec{\Psi}_{\text{out}}\rangle$ as

$$\begin{aligned} |\vec{\Psi}_{\text{out}}\rangle &= H_{\text{LC},N}H_{\text{LC},N-1}\cdots H_{\text{LC},2}H_{\text{LC},1}|\vec{\Psi}_{\text{in}}\rangle \\ &= \prod_{m=1}^{N} H_{\text{LC},m}|\vec{\Psi}_{\text{in}}\rangle. \end{aligned} \tag{12}$$

For polarization-independent phase modulation, the outgoing light field should be identical to the incident light field, but has an extra optical phase Φ. That means

$$\prod_{m=1}^{N} H_{\text{LC},m} = e^{j\Phi}\begin{bmatrix} 1 & 0 \\ 0 & 1 \end{bmatrix}. \tag{13}$$

From Eqs. (12) and (13), the set of wave plates thus functions as a polarization-independent phase modulator as expressed in Eq. (14):

$$|\vec{\Psi}_{\text{out}}\rangle = e^{j\Phi}|\vec{\Psi}_{\text{in}}\rangle. \tag{14}$$

Assume we have two LC wave plates and the fast axis of the first LC wave plate is parallel to the x axis and the fast axis of the second LC wave plate is perpendicular to the x axis, which means the fast axes of the two LC wave plates are orthogonal to each other. On application of a voltage, LC molecules rotate in the y-z plane and the x-z plane for the first wave plate and the second wave plate, respectively.

Then

$$H_{\mathrm{LC},2}H_{\mathrm{LC},1} = e^{j(\tilde{\phi}_1+\tilde{\phi}_2)}\begin{bmatrix} e^{-j(\Gamma_1-\Gamma_2)/2} & 0 \\ 0 & e^{j(\Gamma_1-\Gamma_2)/2} \end{bmatrix}. \quad (15)$$

Pure optical phase modulation requires $\Gamma_1 = \Gamma_2$, which leads to

$$(n_{\mathrm{eff},1} - n_{o,1})d_1 = (n_{\mathrm{eff},2} - n_{o,2})d_2, \quad (16)$$

where $n_{\mathrm{eff},i}$ and $n_{o,i}$ $(i = 1, 2)$ are the effective extraordinary refractive index and the ordinary refractive index of the two LC wave plates, respectively. $n_{\mathrm{eff},i}$ depends on the applied electric field, but $n_{o,i}$ is independent of the electric field. The optical phase ϕ is given by

$$\phi = \tilde{\phi}_1 + \tilde{\phi}_2 = \frac{k_0}{2}[(n_{\mathrm{eff},1} + n_{o,1})d_1 + (n_{\mathrm{eff},2} + n_{o,2})d_2]. \quad (17)$$

To further simplify Eqs. (16) and (17), we assume that the two LC wave plates are identical. That is, $d_1 = d_2 \equiv d$, $n_{\mathrm{eff},1} = n_{\mathrm{eff},2} \equiv n_{\mathrm{eff}}$, and $n_{o,1} = n_{o,2} \equiv n_o$. As a result, Eq. (17) becomes

$$\phi(V) = k_0(n_{\mathrm{eff}}(V) + n_o)d. \quad (18)$$

From Eq. (12),

$$|\vec{\Psi}_{\mathrm{out}}\rangle = e^{j\phi(V)}|\vec{\Psi}_{\mathrm{in}}\rangle = e^{jk_0(n_{\mathrm{eff}}(V)+n_o)d}|\vec{\Psi}_{\mathrm{in}}\rangle. \quad (19)$$

Equation (19) means that the two orthogonal LC wave plates function as a polarization-independent LC phase modulator whose optical phase is electrically tunable. The optical phase difference $\Delta\phi$ between V and $V = 0$ is then expressed as

$$\Delta\phi = \phi(V) - \phi(0) = k_0(n_{\mathrm{eff}}(V) - n_{\mathrm{eff}}(0))d. \quad (20)$$

Assume the two orthogonal LC wave plates are initially aligned parallel along the x or y direction, and LC directors with positive dielectric anisotropy tend to be reoriented along the z direction. When the applied voltage is much larger than the threshold voltage V_{th}, $n_{\mathrm{eff}}(0) = n_e$ and $n_{\mathrm{eff}}(V) \sim n_o$. Therefore, Eq. (20) becomes

$$|\Delta\phi| = k_0|n_e - n_o|d = \frac{2\pi}{\lambda}|n_e - n_o|d. \quad (21)$$

Equation (21) indicates that the maximum of the tunable polarization-independent optical phase depends on the birefringence of the nematic LC, the wavelength, and the thickness of the LC wave plate.

We further extend the concept of LC phase modulation to LC lenses. To design a polarization-independent LC lens, the exponential phase term $e^{j\Phi}$ in Eq. (14) of the lens's transmittance function must correspond to the desired lens configuration. The optical phase Φ equals $k_0W(r)$, where $W(r)$ is the path length error (or so-called wavefront function) at the point r. Furthermore, the wavefront function $W(r) = n(r)d$, where $n(r)$ is the refractive index at r. Assume $W(r)$ can be decomposed into the following series:

$$W(r) = \sum_{m=0}^{\infty} a_m r^m \mathrm{rect}\left(\frac{r}{2r_0}\right), \quad (22)$$

$$\mathrm{rect}\left(\frac{r}{2r_0}\right) = \begin{cases} 1, & |r| \le r_0, \\ 0, & |r| > r_0, \end{cases} \quad (23)$$

where a_m is a constant for the mth order and the aperture size is $2r_0$. Assume $W(r)$ is a convergent function and $W(r) = 0$ at $|r| = r_0$. The lens power $P(r)$ in the unit of diopters, the inverse of the focal length, is defined as [24]

$$P(r) = \frac{-1}{r}\frac{\partial W(r)}{\partial r}. \quad (24)$$

From Eqs. (21)–(24), $P(r)$ can be expressed as

$$P(r) = -\sum_{m=1}^{\infty} a_m m r^{m-2}\mathrm{rect}\left(\frac{r}{2r_0}\right) = \frac{-d}{r}\frac{\partial n(r)}{\partial r}. \quad (25)$$

Equation (25) indicates two things: The first is that the lens power is position dependent as the wavefront is, generally speaking, an arbitrary function. In ophthalmic applications, a lens with position-dependent lens power is called a "progressive lens." The second one is that such as a position-dependent lens power depends on the first derivative of $n(r)$ related to LC molecule orientation at r. Assume $W(r)$ is a parabola (parabolic approximation): $W(r)_{\mathrm{para}} = d((n_b - n_c)/{r_0}^2)r^2$, where n_b and n_c are the refractive indices in the peripheral region and the central region of the lens, respectively, r_0 is the radius of the aperture, and d is the lens thickness. As a result, the lens power under the parabolic approximation is independent of r:

$$P_{\mathrm{para}} = \frac{-2d(n_b - n_c)}{{r_0}^2}. \quad (26)$$

The maximum of $n_b - n_c$ is the birefringence of a nematic LC (i.e., $\Delta n = n_e - n_o$). A polarization-independent LC lens is characterized by a polarization-independent refractive index function $n(r)$. To realize a polarization-independent LC lens, the architecture can be based on the stacking of many LC wave plates together to have the polarization-independent optical phase in Eq. (14). Then proper design of the distribution of the polarization-independent optical phase and the transmittance function of the architecture would result in a polarization-independent lens. The simplest architecture is based on double-layered LC wave plates. The commonly realized devices are presented as

two identical LC GRIN lenses with orthogonal orientations [10–12,21–23].

Let us estimate how big the optical power could be in both the positive lens regime and the negative lens regime. To do this, we need to find the LC director profile $\tilde{\theta}(r, V)$. The LC director profile is determined by the minimum of the total free energy:

$$F = F_{\text{elastic}} + F_{\text{electric}} + F_S, \tag{27}$$

where

$$F_{\text{elastic}} = \frac{1}{2}K_{11}\int (\text{div}\,\mathbf{n})^2 dV + \frac{1}{2}K_{22}\int (\mathbf{n}\cdot\text{curl}\,\mathbf{n})^2 dV + \frac{1}{2}K_{33}\int (\mathbf{n}\times\text{curl}\,\mathbf{n})^2 dV$$

is the LC elastic free energy where, $\mathbf{n}$ is the LC director,

$$F_{\text{electric}} = -\frac{1}{2}\varepsilon_0\varepsilon_a\int (\mathbf{n}\cdot\mathbf{E})^2 dV \tag{28}$$

is the LC interaction with the external electric field, and the surface term is given by

$$F_S = -\frac{1}{2}W\int (\mathbf{n}\cdot\mathbf{e})^2 dS \tag{29}$$

K_{ii} is the LC elastic constant, ε_a is the electric anisotropy at the frequency of the applied electric field, $\mathbf{E}$ is the externally applied electric field, $\mathbf{e}$ is the easy axis direction, and W is the anchoring energy of the LC director at cell bounding substrates.

The minimization of the total free energy results in the following Euler-Lagrange equation:

$$\theta_{zz}(K_{33}\sin^2\theta + K_{11}\cos^2\theta) + \theta_z{}^2(K_{33} - K_{11})\sin\theta\cos\theta + \varepsilon_0\varepsilon_a E_z^2\sin\theta\cos\theta = 0. \tag{30}$$

Since the characteristic size of the LC director inhomogeneity in the z direction (cell thickness $L = 50$ μm) is much smaller than the characteristic size of the director inhomogeneity in the x and y directions (lens aperture $r_0 = 5$ mm) we ignored the derivatives with respect to x and y compared with the derivatives with respect to z. For simplicity, we assume there is strong director anchoring at LC slab boundaries: $\theta(z = 0) = \theta(z = L) = \text{const}$.

The simulated LC lens consists of two indium tin oxide (ITO) electrodes separated by an insulating layer. The first ITO electrode features a 10-mm-diameter hole pattern coated with a high-resistivity layer, while the second ITO electrode is a continuous ITO film. The driving voltages V_1 and V_2 are applied to the first and second electrodes, respectively. A third ITO film, isolated from the patterned electrode by the LC layer and a buffering layer, is held at ground potential. The ac electric field satisfies the equation

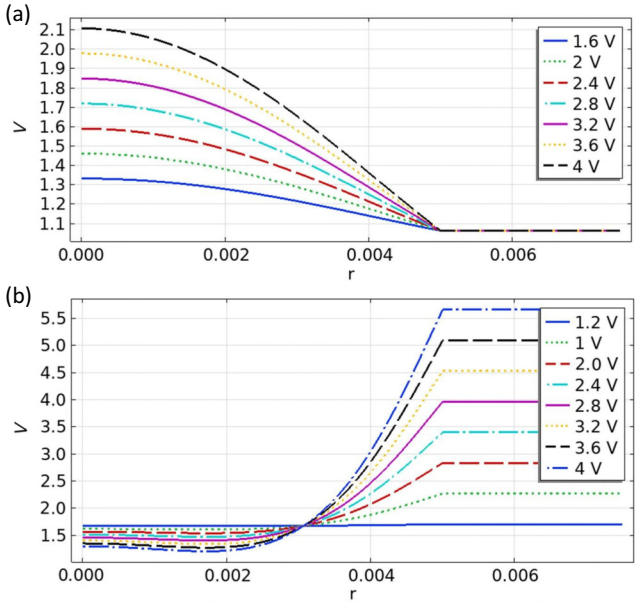

FIG. 2. Electric potential at the top of the LC layer for positive and negative lenses at different applied voltages V_1 and V_2. (a) $V(z = L)$ for a positive lens at $V_1 = 1.2$–4 V and $V_2 = 1.2$ V. (b) $V(z = L)$ for a negative lens at $V_1 = 0.75$ V and $V_2 = 1.2$–4 V.

$$\nabla\cdot\mathbf{j} = 0,\ \mathbf{j} = \sigma\mathbf{E} + i\omega\mathbf{D} \tag{31}$$

with the appropriate boundary conditions for the electric potential U at the bottom electrode (ground electrode), hole electrode (V_1), and top electrode (V_2), $\mathbf{E} = -\nabla U$. Here $\mathbf{D}$ is the electric displacement vector, $\mathbf{D} = \varepsilon_0\hat{\varepsilon}\mathbf{E}$, $\varepsilon_{ij} = \varepsilon_\perp\delta_{ij} + (\varepsilon_{||} - \varepsilon_\perp)n_i n_j$, σ is the ac conductivity of high-resistivity layer, and ω is the frequency of the applied ac field. Equations (30) and (31) are coupled via the LC director angle θ. In Fig. 2 we present the electric potential at the top of the LC layer for positive [Fig. 2(a)] and negative [Fig. 2(b)] lenses at different applied voltages V_1 and V_2. The optical path differences (OPDs) for a normally incident plane wave passing through the LC layer in the positive and negative lens regimes are depicted in Figs. 3(a) and 3(b). One can estimate the expected optical power for positive and negative lenses by using the equation

$$P = 2\frac{W_{\text{OPD}}(r = 0) - W_{\text{OPD}}(r = r_0)}{r_0{}^2},$$

which results in the optical power for the positive lens $P_{\text{positive}} \sim 0.9D$ at $V_1 = 4$ V and $V_2 = 1.2$ V and $P_{\text{negative}} \sim -0.92D$ for the negative lens at $V_1 = 0.75$ V and $V_2 = 4$ V.

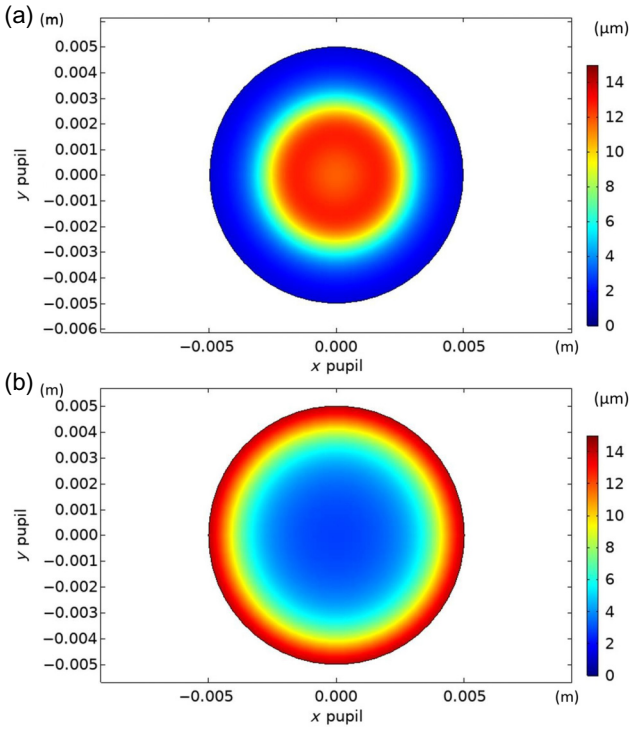

FIG. 3. W_{OPD} in positive and negative lens regimes. (a) Positive lens: $V_1 = 4$ V and $V_2 = 1.2$ V. (b) Negative lens: $V_1 = 0.75$ V and $V_2 = 4$ V.

III. EXPERIMENTAL RESULTS AND DISCUSSION

A. Sample fabrication

The top view and the side view of the LC electronic lens are illustrated in Figs. 4(a) and 4(d), respectively. Two identical LC cells are bonded together with the use of optically clear adhesive. The LC electronic lens is 51×31 mm^2, with an active lens region measuring 10 mm. Without an applied electric field, the rodlike LC molecules in the top and bottom LC layers are aligned orthogonally: the top LC layer is oriented in the x direction, while the bottom LC layer is oriented in the y direction [Fig. 4(a)]. When we apply a high enough electric field to the two LC layers in the LC electronic lens, all LC molecules tend to reorient themselves toward the z direction. The lens power in the unit of diopters, defined as the inverse of the focal length, is zero at either no electric field or very high electric field. Each point of the incident plane wave travels at the same light speed, and then the incident plane wave remains a plane wave. This means there is no focusing effect. When the applied electric field is high enough to overcome the LC orientational elasticity subject to the anchoring of LC molecules in the alignment layers [33], the LC molecules start to reorient themselves. The voltage when the LC reorientation starts is called the "threshold voltage" V_{th}. When the applied voltages $V_1 > V_2 > V_{\mathrm{th}}$ and $V_3 > V_4 > V_{\mathrm{th}}$, the LC molecules of both LC layers in the central part of the active lens region are more parallel to the glass substrates, while the LC molecules near the edge of the aperture are more perpendicular to the substrates [Figs. 4(b) and 4(e)]. Across the aperture of the active region, each cross section has a LC molecular distribution. The incident plane wave is then modulated to a converged spherical or parabolic wave when the light travels more slowly at the center than at the edge of the aperture. The LC electronic lens functions as a positive lens. Similarly, when the applied voltages $V_2 > V_1 > V_{\mathrm{th}}$ and $V_4 > V_3 > V_{\mathrm{th}}$, the LC molecules in the central region of both LC layers are more perpendicular to the glass substrates than the ones near the edge of the aperture [Figs. 4(c) and 4(f)]. The LC electronic lens functions as a negative lens. The orientations of the liquid-crystal molecules in the top and bottom LC layers are orthogonal to each other until all the LC molecules tilt upward along the z axis. Thus, the wavefront of the LC electronic lens is not only electrically tunable but is also polarization independent. In other words, the LC electronic lenses are polarization independent.

The manufacturing process was conducted within a generation 3.5 fabrication facility of Innolux Corporation in Taiwan. The substrate glass had a total size of 630×720 mm^2, coated with a patterned ITO layer, which enabled the fabrication of 72 single glass units (size 51×31 mm^2), equivalent to 36 LC electronic lenses, followed by cleaning with deionized water and potassium hydroxide in the cleaning process (not to scale in Fig. 5). After the cleaning process, the ITO substrates were printed with the alignment layers (specifically polyimide, Nissan 7492) to align the LC molecules, and were subjected to a precuring temperature of 75 °C for 30 min and a main curing temperature of 230 °C for 60 min to ensure complete evaporation of solvents from the polyimide. This was followed by a mechanical rubbing of the alignment layer with cotton cloths wrapped on a roller with a roller speed of 1500 rpm. The function of the mechanically rubbed alignment layers is to establish the initial orientation of liquid-crystal molecules, aligning them in a specific direction with a small tilt angle of 1°–2°. Thereafter, spherical spacers with a diameter of 50 μm were uniformly distributed across the substrate at a density of 16 particles/mm^2 for the purpose of maintaining the layer thickness between the two glass substrates. The next step was the printing of the sealing glue with the use of an acrylic adhesive for preparation of the next cell assembly process. Subsequently, another glass substrate was prepared for the assembly process. This substrate was coated with several functional layers in the following order: an ITO layer for electrical conductivity, an insulating layer (SiN_x, thickness 6900 Å) to prevent short circuits, a 10 mm hole-patterned ITO layer, and a high-resistivity layer (sheet resistance approximately 10^7 Ω/□), consisting of indium oxide and silicon dioxide, deposited via sputtering in the designated glass region. This substrate also underwent mechanical

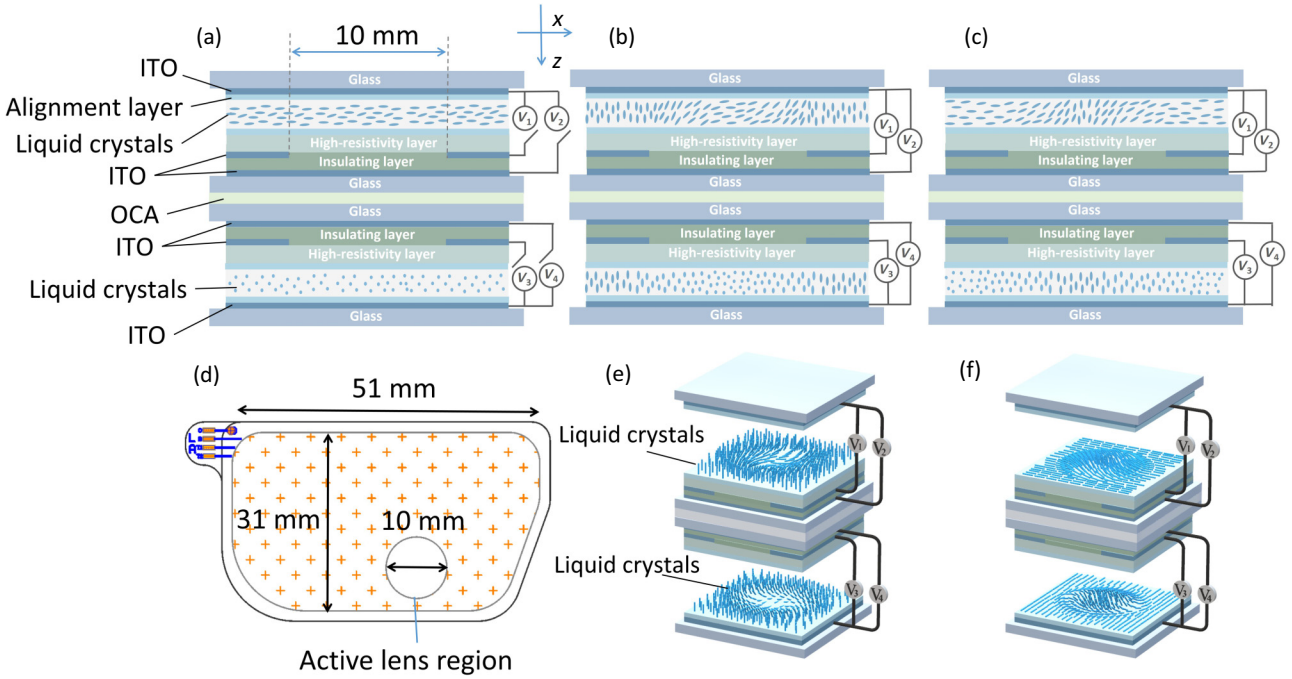

FIG. 4. (a)–(c) Side view and (d) top view of the LC electronic lens based on two orthogonally arranged LC layers. The size is 51×31 mm^2. (a)–(c) Side view near the hole-region in (d). (b),(e) Positive lens when LCs in the central part are more parallel to the glass substrate. (c),(f) Negative lens when LCs in the central part are more perpendicular to the glass substrate. (e),(f) Three-dimensional illustrations of (b),(c), respectively. ITO, indium tin oxide; OCA, optically clear adhesive.

rubbing on its alignment layer, similarly to the first substrate, to ensure proper alignment of the LC molecules. After the precise alignment of the two substrates, they were bonded together at 150 °C for 10 min, ensuring a strong, uniform bond that preserves the alignment layers and spacers. Following the cell assembly process, the bonded substrates were carefully cut into individual lens cells. The nematic liquid crystal (Merck, MLC-2172, $\Delta n = 0.29$, $\Delta\varepsilon = 13.4$, $K_{11} = 13$ pN, $K_{33} = 16.5$ pN) was injected into the lens cells by capillary force. After the LC injection, each lens cell was sealed with the use of an ultraviolet curing adhesive (Norland Optical Adhesive, NOA65) and then exposed to ultraviolet light to ensure an airtight closure.

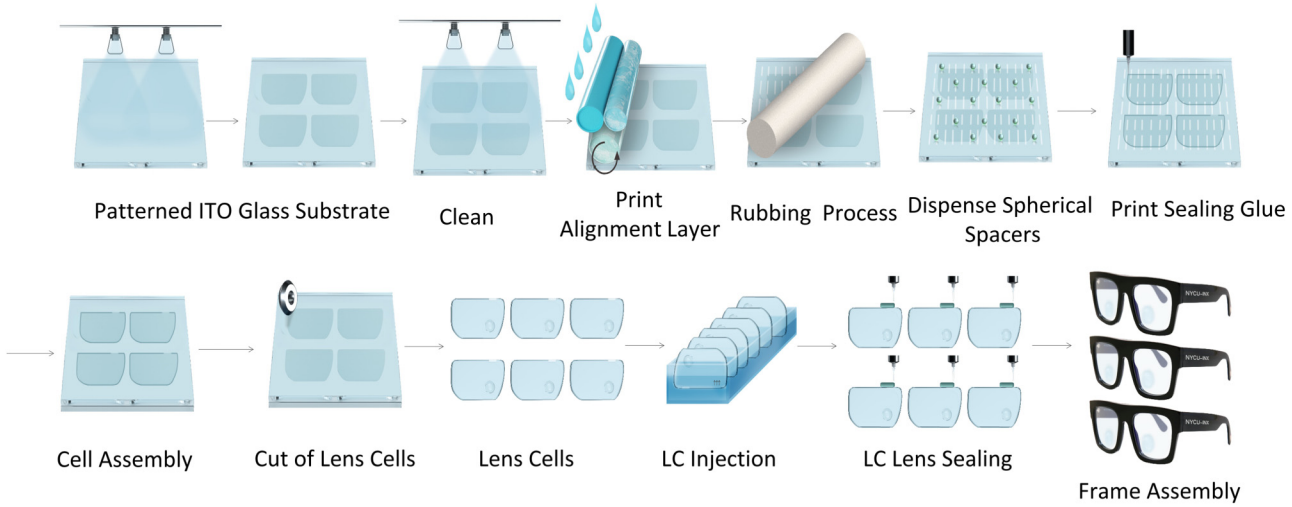

FIG. 5. Manufacturing process for the LC electronic lenses. The size of the substrate glass is 630×720 mm^2, which enables the fabrication of 72 single glass units, equivalent to 36 LC electronic lenses. The drawings are not to scale.

The final assembly involves bonding two LC lenses to form an LC electronic lens, with the rubbing directions of the two LC layers oriented orthogonally to each other. This was done with optically clear adhesive (3M CEF2806, thickness 150 μm). The bonding process was conducted under controlled conditions—roller pressure between 0.1 and 0.2 MPa and roller speed of 1 m/min, followed by a curing step in a chamber at 50 °C under a 3 kg load for 20 min. These steps are designed to eliminate any potential bubble formation in the transparent area of the lens, ensuring flawless optical quality. The LC electronic lens with total thickness of approximately 1.7 mm and weight of 10 g was subsequently integrated into spectacle frames. The electronic components for the LC electronic lens were installed in the temples of the frames. Figure 6(a) shows a photograph of the prototype of LC electronic spectacles based on a LC GRIN lens. Figure 6(b) displays a photograph of an LC electronic lens featuring only a single LC layer. In Fig. 6(c), a person is shown trying on the LC electronic spectacles.

In a comprehensive structure, including lenses and temples with electronics [Fig. 6(d)], the right temple of the eyeglasses consists mainly of a rechargeable battery module, a switch button, and a charging port for the battery. The left temple of the eyeglasses houses the driving control board, with details shown in Fig. 6(e). Figure 6(f) depicts a corresponding functional block diagram of the driving electronics. A lithium-ion battery powers the entire LC electronic spectacle assembly, providing the necessary digital voltage for the operation of the microcontroller unit (MCU; Hycon Tech, HY16F188) and the touch switch module. A gentle touch on the switch button by a human finger changes the capacitance, which is detected by the sensor integrated circuit (SOT-23-6 metal-oxide-semiconductor field-effect transistor) in the touch switch module. This triggers the module to send a signal to the

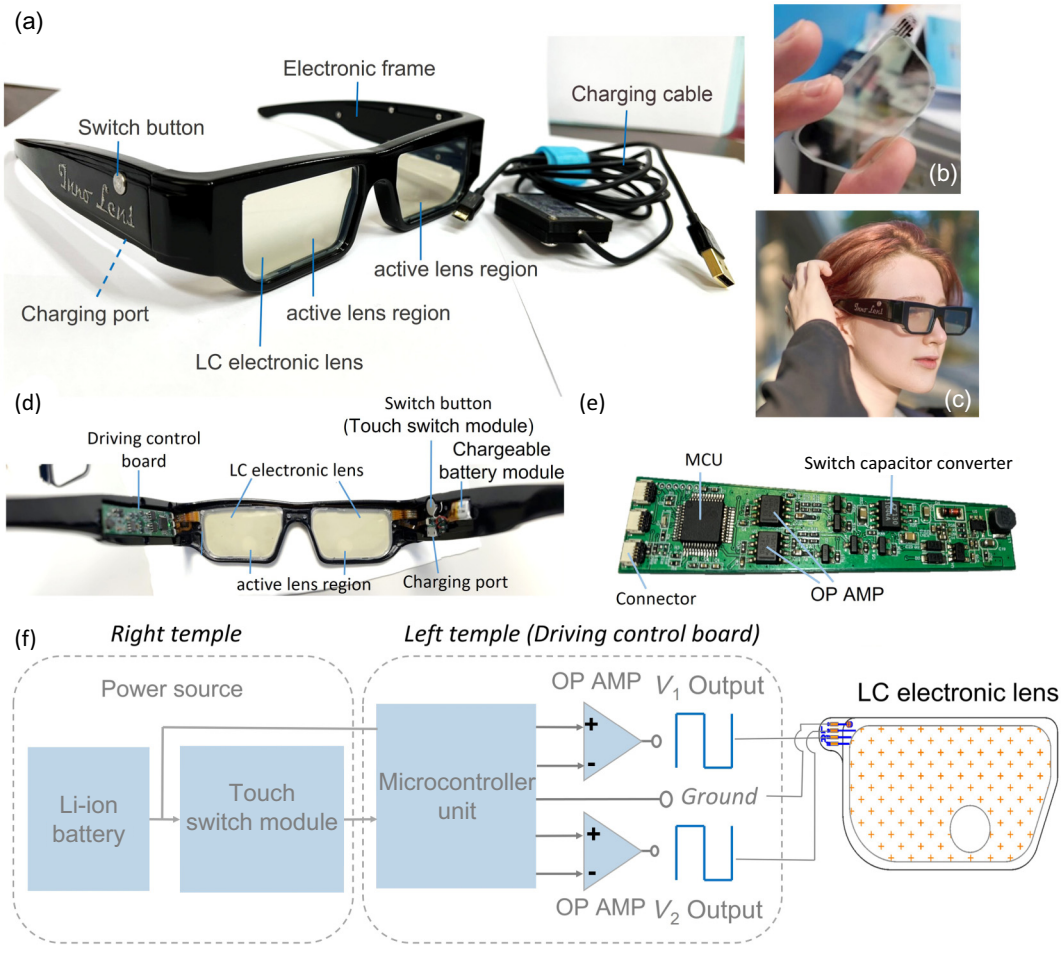

FIG. 6. Design and electronics of fabricated LC electronic spectacles. (a) First prototype of polarizer-free LC electronic spectacles based on LC GRIN lenses and the charging cable. (b) Photograph of a LC electronic lens with only one LC layer. (c) Ms. Mariia Leontieva trying on the first prototype of the polarizer-free LC electronic spectacles. (d) Comprehensive structure of the LC electronic spectacles. (e) Physical driving control board in the left temple in (d). (f) Corresponding functional block diagram of the electronics of the LC electronic spectacles. OP AMP, operational amplifier.

MCU, which then generates output signals for various functions. The voltage signals V_1, V_2, and ground, produced by the MCU and amplified through two operational amplifier circuits, serve as the operational voltages applied to the two LC layers in the LC electronic lens. The control boards in the left and right temples are interconnected by a slim and flexible printed circuit that carries the signal and power lines. The left and right LC electronic lenses both receive the same ac voltages.

B. Electro-optical properties

To test whether the LC electronic lens is polarization independent, we observed the phase profile under crossed polarizers, with the transmission axis of one polarizer set at 45 relative to one of the LC layers at 0 V. Since the LC electronic lens consists of two LC layers, we operated one LC layer at a time while keeping the LC molecules in the other layer aligned perpendicularly to the glass substrate [Figs. 7(a)–7(l)]. The light intensity in Fig. 7(a) represents the phase retardation between two linearly eigenpolarized light components. The adjacent concentric rings indicate a phase retardation of 2π radians, meaning that more rings correspond to greater phase retardation. The phase profiles in Figs. 7(a), 7(d), 7(g), and 7(j) are similar to those in Figs. 7(b), 7(e), 7(h), and 7(k), indicating that the two LC layers exhibit comparable phase profiles. By counting the number of concentric rings in Figs. 7(a), 7(b), 7(d), 7(e), 7(g), 7(h), 7(j), and 7(k) (we calculated the lens power as a function of the applied voltage [Fig. 7(m)]. Each LC layer acts as a polarization-sensitive LC lens, with the lens power ranging from +1D to −1D for each layer. The operating voltage is less than 4 V_{rms} and the operating frequency is less than 530 Hz. The theoretical lens power ranges from approximately +1.16D to approximately −1.16D, and the experimental results are close to these theoretical values. When both LC layers are activated simultaneously and the electric signals are adjusted to achieve similar lens powers in each layer, we barely observe the concentric rings [Figs. 7(c), 7(f), 7(i), and 7(l)]. This indicates that the variation in phase retardation between the two linearly eigenpolarized light components in different parts of the sample is much smaller than that observed in a single LC layer. This also suggests that the LC electronic lens is nearly polarization independent. Theoretically, a polarization-independent phase profile should appear completely dark, with no fringes at all. However, we still observed at most five dark lines across the aperture, indicating a 10π radian or optical path variation of 2.5 μm for $\lambda = 0.5$ μm. The measured thickness of the top LC layer is 62.3 μm and that of the bottom LC layer is 53.1 μm. The cell gap is around 9.2 μm. The estimated optical path variation due to the thickness variation should be around 2.76 μm, which is close to the experimental value (2.5 μm). By adjustment of the voltages of the two LC layers, the lens power of each layer is not only individually adjustable but is also electrically and continuously tunable. Two conditions for the positive lens and the negative lens [Figs. 7(c) and 7(i)] were selected to plot the measured wavefronts at different oscillating angles of linearly polarized light in Fig. 7(n): +1D [top row in Fig. 7(n)] and −1D [bottom row in Fig. 7(n)]. As one can see, the wavefronts at different angles of linearly polarized light are all similar to the wavefront without a polarizer. From Fig. 7(n), we plot the OPD and the calculated lens power as a function of the x pupil coordinate in Figs. 7(o) and 7(p), respectively. The OPDs for the positive and negative lenses show similar patterns, with only small variations at different angles of linearly polarized light [Fig. 7(o)]. The lens power is quite uniform along the x pupil coordinate at $|x| > 0.5$ mm [34,35] with small variation [Fig. 7(p)]. This indicates that the active lens region of the LC electronic lens is polarization independent and functions almost like a single vision lens, exhibiting a constant lens power across the pupil when the radius exceeds 0.5 mm. The measured transmission of the polarization-independent LC electronic lens is approximately 55% at $\lambda = 550$ nm, while the transmission for a single LC lens without a polarizer is around 75% [Fig. 7(q)]. In contrast, the transmission drops to 23% for a single LC lens with a polarizer. To operate a single LC lens (without orthogonal LC layers), it is necessary to use a polarizer that has a transmission of 31% to modulate the extraordinary wave, while filtering out the ordinary wave. The polarizer-free (polarization-independent) LC electronic lens has a benefit in transmission compared with the conventional LC GRIN lens. To further increase transmission, application of an antireflection coating, selection of better materials to minimize absorption in the ITO and polyimide layers, and improvement of refractive index matching between optical layers to reduce interfacial reflection would significantly contribute to boosting transmission. On the other hand, the simulation results in Figs. 7(m), 7(o), and 7(p) show good agreement with the measured results. The minor discrepancies between them can be attributed to our ignoring the influence of the changing capacitor on the electric field due to the realignment of LC directors. The simulation parameters are listed in Table II in the Appendix.

C. Image and response time

To test image performance under ambient light, we directly attached the sample, without any polarizer, to a camera and positioned three targets at distances of 59 cm ("news"), 117 cm (sailing ship on the sea), and 700 cm (hot air balloon over the sea) from the sample [Fig. 8(a)]. The camera (Canon 760D) was used to mimic the human eye. When the sample was set to 0D, we adjusted the camera to focus on the image of the sailing ship on the sea

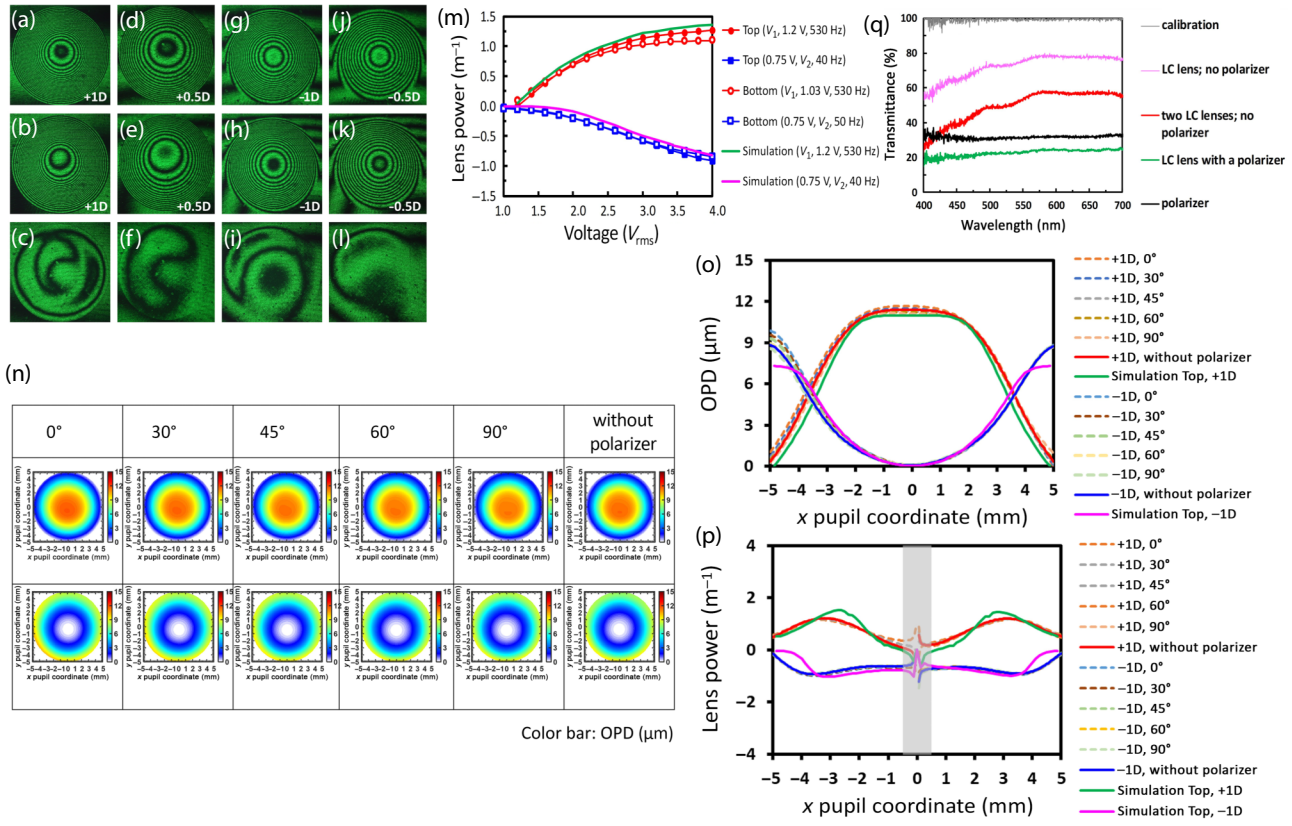

FIG. 7. Electro-optical properties of a LC electronic lens. (a)–(l) Selective phase profiles of the active lens region in a LC electronic lens. Two adjacent concentric rings represent phase retardation of 2π radians. The corresponding voltages and frequencies are listed in Table I in the Appendix. (a),(d),(g),(j) Different voltages are applied to the top LC layer and the same voltages and frequency are applied to the bottom LC layer to align LC molecules along the z axis. This means the phase profiles are contributed by the top LC layer only. (b),(e),(h),(k) Different voltages are applied to the bottom LC layer and the same voltages and frequency are applied to the top LC layer to align LC molecules along the z axis. This means the phase profiles are contributed by the bottom LC layer. (c),(f),(i),(l) Same voltages and frequency applied to the top LC layer as for (a),(d),(g),(j) and same voltages and frequency applied to the bottom LC layer as for (b),(e),(h),(k). In (c),(f),(i),(l) there are almost no concentric rings, which means the phase retardation is small. The LC electronic lens is polarization independent under two mutually orthogonal LC layers. (m) Lens power as a function of voltage. The blue line with filled squares represents the lens power of the top LC layer of the LC electronic lens at different values of V_2 for $V_1 = 0.75$ V_{rms} at 40 Hz. The magenta line corresponds to the simulation results for the top LC layer of the LC electronic lens at different values of V_2 for $V_1 = 0.75$ V_{rms} at 40 Hz. The orange line with filled circles represents the lens power of the top LC layer at different values of V_1 for $V_2 = 1.2$ V_{rms} at 530 Hz. The green line corresponds to the simulation results for the top LC layer of the LC electronic lens at different values of V_1 for $V_2 = 1.2$ V_{rms} at 530 Hz. The blue line with open squares represents the lens power of the bottom LC layer at different values of V_2 for $V_1 = 0.75$ V_{rms} at 50 Hz. The red line with open circles represents the lens power of the bottom LC layer at different values of V_1 for $V_2 = 1.03$ V_{rms} at 530 Hz. The lens powers at the top and bottom LC layers are similar, ranging from -1D to $+1$D. (n) Wavefront measurement at the lens power of $+1$D (top row) and -1D (bottom row) when we rotated the polarizer to different angles. The electrical conditions for $+1$D and -1D are as same as in (c),(i), respectively. The results show wavefronts of the LC electronic lens are polarization independent. The color bar indicates the OPD in the unit of microns. (o) OPD vs x pupil coordinate at different lens powers and oscillation angles of linearly polarized light. The green and magenta lines correspond to the simulation results for the electrical conditions for $+1$D and -1D, respectively. (p) Lens power as a function of x pupil coordinate at different lens powers and oscillation angles of linearly polarized light. The green and magenta lines denote the $+1$D and -1D simulations. (q) Measured spectrum of the LC electronic lens at 0D. The gray line represents the spectrum calibrated by the incident light. The spectra of a single LC lens and two-orthogonal LC lenses without a polarizer are represented by the pink and red lines. The spectra of a polarizer and a LC lens attached with a polarizer are represented by black and green lines.

at 117 cm and took a photograph. The camera mimicked the eye with myopia and presbyopia, so both the distant object and the near object were blurred. Next, we applied electric signals to the LC electronic lens to achieve a lens power of -1D in the active lens region, allowing the camera to capture the distant object: the hot air balloon over the sea at 700 cm. Similarly, the image of the "news" at 59 cm remained clear, as the active lens region was set

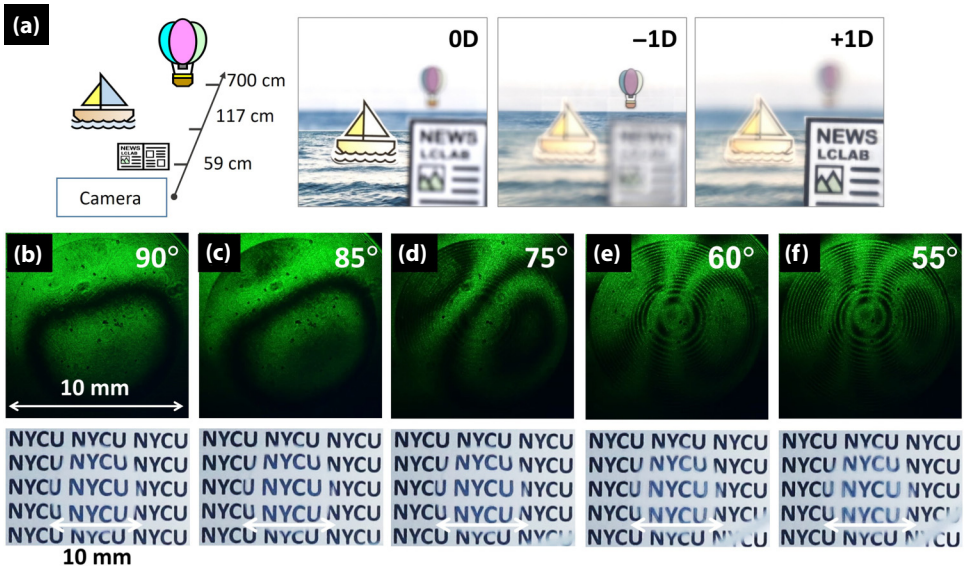

FIG. 8. Image performance of polarizer-free LC electronic lenses. (a) Experimental setup for determining image performance when the LC electronic lens is at 0D, −1D, and +1D. Three targets are placed 59 cm ("news"), 117 cm (sailing ship on sea), and 700 cm (hot air balloon over the sea) from the LC lenses. Photographs are taken under unpolarized ambient light. The active LC region is 10 mm. (b)–(f) Phase profiles and image performance when the rubbing direction of the two LC layers changes from 90° to 55°. The LC lenses are operated at a lens power of +1D. The LC active region is 10 mm.

to +1D. Theoretically, the two LC layers should be identical and mutually orthogonally aligned. However, errors and differences are inevitable in practice, especially during mass production. What tolerance should we maintain for such differences? When the two LC layers are not perfectly orthogonal [Figs. 8(b)–8(f), for example, ranging from 90° to 55°], we observed that vague concentric rings appear when the angle between the two LC layers drops below 80°, and the image becomes blurrier as the angle decreases. The images look quite similar when the angle is between 90° and 85°. The manufacturing angle tolerance is around 1°, which is less than the experimental tolerance of 5°. This suggests that orthogonal LC layers are manufacturable. As the angle becomes increasingly nonorthogonal, the polarization becomes less independent. If we assume that the angle between the alignments of the two LC layers is $(90-\theta)°$ and we use the small-angle approximation of θ, Eq. (14) should be modified as

$$\left|\vec{\Psi}_{\text{out}}\right\rangle = e^{j\Phi}\begin{bmatrix} 1 & \theta(1-e^{j\Gamma}) \\ -\theta(1-e^{-j\Gamma}) & 1 \end{bmatrix}\left|\vec{\Psi}_{\text{in}}\right\rangle. \quad (32)$$

When θ increases, phase retardation of the LC layers occurs, and that is why we observe the vague concentric rings in Figs. 8(d)–8(f).

To study the chromatic properties of the lenses, collimated and incoherent white light, along with red or green filters, was shone at the active region of the LC electronic lens with a beam size of 10 mm. The distance between the focal lengths of red and green incoherent light is around 3.72 cm for the LC electronic lens and 1.15 cm for a glass lens (BK7) with the same lens power. The chromatic aberration of the LC electronic lens is 3.24 times greater than that of the glass lens. In comparison, the focal length difference of the Fresnel-type LC lens for red and green incoherent light is approximately 14.4 cm, which is 4 times larger than that of our LC GRIN lens, and diffraction further degrades the incoherent images [36]. Theoretically, the Abbe number of the glass lens (BK7) is around 64, while that of a nematic liquid crystal (e.g., E7) is 15 for the extraordinary wave and 30 for the ordinary wave. Consequently, the chromatic aberration of a typical nematic LC is 2.13 times greater for the extraordinary wave and 4.26 times greater for the ordinary wave in comparison with a glass lens. The LC electronic lens averages the chromatic aberration of the nematic LC, which is another advantage of orthogonal LC layers.

The response time depends on how the electric signals are applied. Here we demonstrate two types of operation of the LC electronic lens for measuring the response time. In the experiments, three targets are positioned at distances of 42, 30, and 22.8 cm from the LC electronic lens [Fig. 9(a)]. The timer is located at 30 cm parallel to one of the objects. Initially, we adjusted the camera to see the object at 30 cm. One operational regime involves aligning the LC molecules perpendicular to the glass substrates at 0D at 0 s by application of different voltages and frequencies [Fig. 9(b)]. The blue-dotted circle indicates the active region of the LC electronic lens. After the LC electronic lens is switched to +1D and −1D, the images at

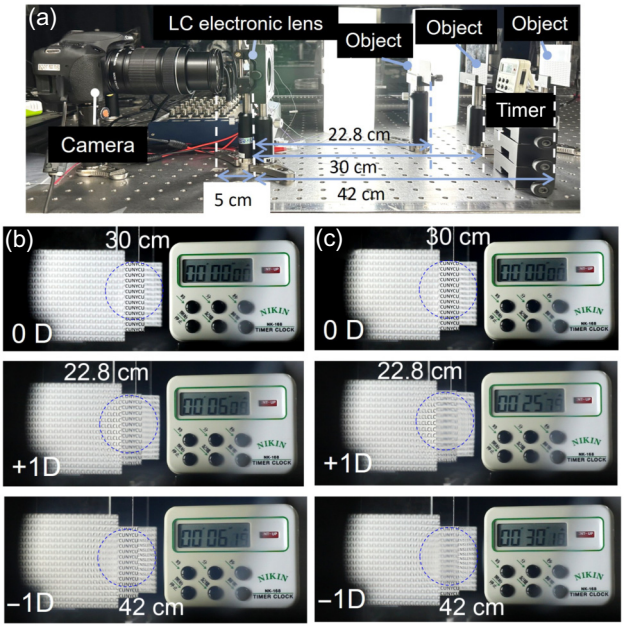

FIG. 9. Response time of polarizer-free LC electronic lenses. (a) The experimental setup for response time measurement. Three targets are placed 42, 30, and 22.8 cm from the LC electronic lenses. The timer is located at 30 cm. (b) The object at 30 cm is clear as the LC molecules are all perpendicular to the glass substrates at 0D at 0 s. The blue-dotted circle represents the active region of the LC electronic lens. After we switched the LC electronic lens to +1D and −1D, the images at 22.8 and 42 cm became clear at approximately 5 s for +1D and at approximately 6 s for −1D. (c) The LC molecules are all parallel to the glass substrates at 0D at 0 s. After we switched the LC electronic lens to +1D and −1D, the images at 22.8 and 42 cm became clear at approximately 25 s for +1D and at approximately 30 s for −1D. The photographs are taken under unpolarized ambient light [37].

22.8 and 42 cm become clear in approximately 5 s for +1D and in around 6 s for −1D. The other operational regime has the LC molecules aligned parallel to the glass substrates at 0D at 0 s without application of any voltages [Fig. 9(c)]. We then switched the LC electronic lens to +1D and −1D, and the images at 22.8 and 42 cm are clear at approximately 25 s for +1D and at approximately 30 s for −1D. The response time changes by approximately 6 times with different electric operations. When we turn off the electric fields applied to the LC layers, the response time depends primarily on the relaxation of the LC molecules, which is related to the elastic properties of nematic liquid crystals (viscosity, elastic constant, and birefringence) [33]. However, the response time of the LC layers is 5 times faster when we operate between two types of operations, as the application of an electric field to the LC layers enhances the response of the LC molecules and helps suppress damping relaxation. This explains the variation in response time under different electrical modes of operation. To further reduce the response time, the optimization driving scheme needs to be designed for practical applications. The implementation of a bilayer LC structure to achieve polarization-free operation was first proposed in a patent in 1980 [38]. After that, many researchers adopted the same idea or extended the idea as orthogonally LC molecular alignment for proof of the concept without any rigorous mathematical proof [8–10,19,21,22,25–29]. The results in this paper are a confirmation that the devices have the desired properties as built, more than a proof of the operating principle.

IV. CONCLUSION

The advantages of the demonstrated LC electronic lenses are polarization independence and electrically tunable wavefronts and lens power. The lenses exhibit acceptable levels of chromatic aberration. It is crucial that the lenses can be manufacturable and industry-ready, marking a significant advancement in the field. However, it is important to acknowledge that the LC electronic spectacles developed still have various weaknesses that require further exploration, such as the response time and aperture size. Human vision can be split into foveal vision and peripheral vision. For the vision to recognize symbols or shapes, the angle is around ±20°. The typical distance between eyeglasses and the eye is around 12 mm. The calculated aperture size for the active LC lens region is then 8.7 mm. Thus, an aperture size of 10 mm should be sufficient [30,39–41]. To further enlarge the aperture, a spatially extended method could be adopted [24]. Instead of using a single active aperture, we could design several smaller active regions, with the active region selectively determined by signals from the eye tracking system. Additionally, to expand the tunable range of lens power, combining the LC lens with a prescription lens could be an effective option. Regarding polarization-independent phase modulation, the principles can be further extended to various arrangements of LC molecules. For instance, one could design LC devices that function as Pauli matrices from a mathematical point of view. The cascading of several Pauli LC devices could create a polarization-independent LC phase modulator for incoming light. From a chemical standpoint, self-orthogonal nematic LC molecules, arranged similarly to the leaves of St. John's wort, are expected to enhance the performance of LC electronic spectacles. To fabricate curved LC lenses, polymeric materials (plastic substrate) should be used to replace the glass substrate. The anticipated challenges include how to achieve the same level of fabrication quality at lower temperatures. Additionally, making two-dimensional curved plastic LC lenses presents significant challenges as well. We believe this study represents a significant milestone not only in the historical evolution of human spectacles but also in the advancement of optical systems.

ACKNOWLEDGMENTS

The authors are indebted to Mr. Chang-Nien Mao (National Yang Ming Chiao Tung University) for technical assistance. This work is supported by the National Science and Technology Council (Taiwan) under Grant No. 114-2112-M-A49-011 and Innolux Corporation. As to commercial relationships disclosure, the principal investigator, Prof. Yi-Hsin Lin, deeply appreciates the unrestricted support from Google through the Google Gift. Google Gift is typically awarded to individual faculty members or research groups based on internal nomination by Google researchers to support academic research. Y.-H. Lin, H.-H. H., W.-C. C., T.-W. H. and V. R. received funding supports from Innolux Corporation. C.-C. C., M.-W. J., C.-L. L., Y.-S. T., Y.-H. W., and C.-L. Y. are employed by Innolux Corporation.

DATA AVAILABILITY

The data underlying the results presented in this paper are not publicly available at this time but may be obtained from the authors upon reasonable request [42].

APPENDIX

1. Measurement of phase profiles

To study the phase profiles of the active lens region of the LC electronic lens, the LC samples were placed between two crossed polarizers individually and the rubbing direction of the LC layers was 45° with respect to one of the polarizers. Images of the LC sample at different voltages and frequencies were recorded by a camera, as shown in Figs. 7(a)–7(l). The corresponding voltages and frequencies for Fig. 7 are listed in Table I. The light transmission T represents the phase retardation Γ between the extraordinary wave and the ordinary wave of entering light, which is expressed as $T = \sin^2(\Gamma/2)$, where $\Gamma = 2\pi(n_{\text{eff}}(V) - n_{\text{o}})d/\lambda$, where n_o is the ordinary refractive index, $n_{\text{eff}}(V)$ is the voltage-dependent effective refractive index of the extraordinary wave, d is the cell gap, and λ is the wavelength. The maximum of $n_{\text{eff}}(V)$ is n_e, the extraordinary refractive index of the nematic LC. Two adjacent bright rings represent phase retardation of 2π radians. From the number of concentric rings, we plot the phase profiles as a function of the pupil coordinate and then calculate the lens power in the unit of diopters, or reciprocal meters, according to Eq. (22). Each LC sample consists of two LC layers [Fig. 2(b)]. To measure the phase profile of each LC layer, we applied different voltages and frequencies to one LC layer, while the LC molecules in the other LC layer were perpendicular to the glass substrate. Figures 7(a), 7(d), 7(g), and 7(j) correspond to the top LC sample with different voltages applied and with the following sample voltages and frequency applied to the bottom LC sample: $(V_3, V_4, f_{34}) = (7\ \text{V}_{\text{rms}}, 7\ \text{V}_{\text{rms}}, 200\ \text{Hz})$. Similarly, Figs. 7(b), 7(e), 7(h), and 7(k), correspond to the bottom LC sample with different voltages applied and with the following sample voltages and frequency applied to the top LC sample: $(V_1, V_2, f_{12}) = (7\ \text{V}_{\text{rms}}, 7\ \text{V}_{\text{rms}}, 200\ \text{Hz})$.

2. Voltage and frequency conditions for Figs. 7(a)–7(l)

Table I lists the voltage and frequency conditions for Figs. 7(a)–7(l). V_1 and V_2 are applied at the same frequency, denoted as f_{12}, while V_3 and V_4 are applied at the same frequency, denoted as f_{34}.

3. Parameters in the simulation

Table II summarizes the structural components of LC lens in the simulation, including the LC layer, hole-patterned ITO electrode, insulating layer, and ground ITO electrode. The layer thicknesses and dielectric constants are the common parameters across these structures. For the LC layer, the governing parameters include the dielectric anisotropy, dielectric constant, conductivity, pretilt angle at boundary and anchoring energy at the boundary. For the electrode layers, the primary governing parameter is

TABLE I. The operating conditions of the two LC lenses in Figs. 7(a)–7(I).

	(V_1, V_2, f_{12})	(V_3, V_4, f_{34})
Figure 7(a)	(2.5 V_{rms}, 1.2 V_{rms}, 530 Hz)	(7 V_{rms}, 7 V_{rms}, 200 Hz)
Figure 7(b)	(7 V_{rms}, 7 V_{rms}, 200 Hz)	(2.75 V_{rms}, 1.03 V_{rms}, 530 Hz)
Figure 7(c)	(2.5 V_{rms}, 1.2 V_{rms}, 530 Hz)	(2.75 V_{rms}, 1.03 V_{rms}, 530 Hz)
Figure 7(d)	(1.72 V_{rms}, 1.2 V_{rms}, 530 Hz)	(7 V_{rms}, 7 V_{rms}, 200 Hz)
Figure 7(e)	(7 V_{rms}, 7 V_{rms}, 200 Hz)	(1.72 V_{rms}, 1.03 V_{rms}, 530 Hz)
Figure 7(f)	(1.72 V_{rms}, 1.2 V_{rms}, 530 Hz)	(1.72 V_{rms}, 1.03 V_{rms}, 530 Hz)
Figure 7(g)	(0.75 V_{rms}, 3.4 V_{rms}, 40 Hz)	(7 V_{rms}, 7 V_{rms}, 200 Hz)
Figure 7(h)	(7 V_{rms}, 7 V_{rms}, 200 Hz)	(0.75 V_{rms}, 3.45 V_{rms}, 50 Hz)
Figure 7(i)	(0.75 V_{rms}, 3.4 V_{rms}, 40 Hz)	(0.75 V_{rms}, 3.45 V_{rms}, 50 Hz)
Figure 7(j)	(0.75 V_{rms}, 2.45 V_{rms}, 40 Hz)	(7 V_{rms}, 7 V_{rms}, 200 Hz)
Figure 7(k)	(7 V_{rms}, 7 V_{rms}, 200 Hz)	(0.75 V_{rms}, 2.81 V_{rms}, 50 Hz)
Figure 7(l)	(0.75 V_{rms}, 2.45 V_{rms}, 40 Hz)	(0.75 V_{rms}, 2.81 V_{rms}, 50 Hz)

TABLE II. The parameters used in the simulation of the LC lens.

Structure	Parameter	Value
Liquid-crystal layer (MLC-2172, Merck)	Dielectric anisotropy $\Delta\varepsilon$	13.4
	Dielectric constant $\varepsilon_\perp$	4.4
	Elastic constant K_{11}	13 pN
	Elastic constant K_{33}	16.5 pN
	n_e	1.52
	n_o	1.8139
	Layer thickness	50 μm
	Conductivity σ_{LC}	5×10^{-15} S/m
	Pretilt angle at boundary	1°
	Anchoring energy at boundary	10^{-4} J/m^2
Hole-patterned ITO electrode	Diameter	10 mm
	Layer thickness	85 nm
	Conductivity σ_{ITO}	4.29×10^5 S/m
	Dielectric constant	9
Insulating layer	Layer thickness	690 nm
	Dielectric constant	7
Ground ITO electrode	Layer thickness	110 nm
	Conductivity σ_{ITO}	4.29×10^5 S/m
	Dielectric constant	9
High-resistivity layer	Layer thickness	38 nm
	Dielectric constant	3.7
	Conductivity σ_{HRL}	1.935 S/m
Operating signal	Frequency	530 or 40 Hz

their electrical conductivity. The hole-patterned ITO electrode has a diameter of 10 mm, and the operating signal frequency is either 530 Hz or 40 Hz.

4. Wavefront measurement

The wavefronts were measured by a Shack-Hartmann wavefront sensor after the beam had propagated through the active lens region of the LC electronic lens [21–23]. The experimental setup includes a light source (He-Ne laser, model 30990, Research Electro-Optics, Inc., $\lambda = 633$ nm), a single-mode fiber, a solid lens with a focal length of 75.6 cm for beam collimation, a pair of solid lenses as relay optics (focal length 14.3 and 6.25 cm), and a wavefront sensor (Thorlabs, WFS150-7AR). The light source was coupled into the single-mode fiber. When light exits from the other end of the fiber located at the focal plane of the lens, collimated light was obtained after the collimating lens. The sample, relay optics, and wavefront sensor were placed in order behind the collimating lens. The distance between the sample and the relay optics was the focal length of the first solid lens of the relay optics. The distance between the wavefront sensor and the relay optics was the back focal length of the second lens of the relay optics. The modulated wavefront immediately after the sample was measured by the wavefront sensor. We reconstructed the wavefronts by Zernike polynomials and obtained the corresponding Zernike coefficients.

5. Spectrum

The spectrum was measured by a spectrometer (Ocean Optics, USB2000+). The range of the light source (MICROTECH, Axen L-150W) is 365–885 nm.

6. Measurement of chromatic properties

To study the chromatic properties of the lenses, incoherent white light with color filters (red or green) was placed in front of a lens (BK7) with a focal length f of 150 mm. After we had placed the LC sample of +1D lens power 30.2 cm behind this lens, we found the minimum spots behind the LC sample and recorded the corresponding positions for green and red light. In comparison, we also studied a lens with a focal length of 1000 mm (or lens power of +1D) and did the same measurement.

7. Measurement of response time

Three targets were placed 42, 30, and 22.8 away from the LC electronic lens [Fig. 5(a)], and the timer was located at 30 cm parallel to one of the objects. At 0 s, the camera was adjusted to see the object at 30 cm. We applied electric signals to the sample, turned on the timer, and recorded a video at the same time. By observing the changes of the image plane, we estimated the response time of the samples.

[1] A. Tbakhi and S. S. Amr, Ibn Al-Haytham: Father of modern optics, Ann. Saudi. Med. **27** (6), 464 (2007).

[2] S. Paetrow, *Besser Sehen: Die Carl Zeiss Augenoptik 1912-2012* (Carl Zeiss Archives, Oberkochen, 2012).

[3] A. M. Smith, Optics to the time of Kepler, Encycl. Hist. Sci. (2022).

[4] C. E. Letocha, The invention and early manufacture of bifocals, Surv. Ophthalmol. **35** (3), 226 (1990).

[5] B. Cretin-Maitenaz, Multifocal lens having a locally variable power, US Patent US2869422A (1959).

[6] P. Kelley, G. Agrawal, M. Bass, J. Hecht, and C. Stroud, *OSA Century of Optics* (The Optical Society, Washington, DC, 2015).

[7] S. Sato, Liquid-crystal lens-cells with variable focal length, Jpn. J. Appl. Phys. **18**, 1679 (1979).

[8] S. Sato, A. Sugiyama, and R. Sato, Variable-focus liquid-crystal Fresnel lens, Jpn. J. Appl. Phys. **24**, L626 (1985).

[9] G. Li, D. L. Mathine, P. Valley, P. Ayras, J. N. Haddock, M. S. Giridhar, G. Williby, J. Schwiegerling, G. R. Meredith,

B. Kippelen, S. Honkanen, and N. Peyghambarian, Switchable electro-optic diffractive lens with highefficiency for ophthalmic applications, Proc. Natl. Acad. Sci. U. S. A. **103** (16), 6100 (2006).
[10] Y. H. Lin, Y. J. Wang, and V. Reshetnyak, Liquid crystal lenses with tunable focal length, Liq. Cryst. Rev. **5** (2), 111 (2017).
[11] H. C. Lin, M. S. Chen, and Y. H. Lin, A review of electrically tunable focusing liquid crystal lenses, Trans. Electr. Electron. Mater. **12** (6), 234 (2011).
[12] L. Li, D. Bryant, and P. J. Bos, Liquid crystal lens with concentric electrodes and inter-electrode resistors, Liq. Cryst. Rev. **2** (2), 130 (2014).
[13] J. W. Goodman, *Introduction to Fourier Optics*, 3rd ed. (Roberts and Company Publishers, Englewood, CO, 2004).
[14] M. G. Douali and J. D. Silver, Self-optimised vision correction with adaptive spectacle lenses in developing countries, Ophthal. Physiol. Opt. **24**, 234 (2004).
[15] B. Bergea and J. Peseux, Variable focal lens controlled by an external voltage: An application of electrowetting, Eur. Phys. J. E **3**, 159 (2000).
[16] L. Chen, M. Ghilardi, J. J. C. Busfield, and F. Carpi, Electrically tunable lenses: A review, Front. Robot. AI **8**, 749005 (2021).
[17] L. W. Alvarez and W. E. Humphrey, Variable power lens and system, US Patent 3,507,565 (1970).
[18] L. W. Alvarez, Development of variable- focus lenses and a new refractor, J. Am. Optom. Assoc. **49** (1), 24 (1978).
[19] S. T. Kowel, D. S. Cleverly, and P. G. Kornreich, Focusing by electrical modulation of refraction in a liquid crystal cell, Appl. Opt. **23** (2), 278 (1984).
[20] T. Nose and S. Sato, A liquid crystal microlens obtained with a non-uniform electric field, Liq. Cryst. **5** (5), 1425 (1989).
[21] Y. H. Lin and H. S. Chen, Electrically tunable-focusing and polarizer-free liquid crystal lenses for ophthalmic applications, Opt. Express **21** (8), 9428 (2013).
[22] H. S. Chen, Y. J. Wang, C. M. Chang, and Y. H. Lin, A polarizer-free liquid crystal lens exploiting an embedded multilayered structure, IEEE Photonics Technol. Lett. **27** (8), 899 (2015).
[23] Y. J. Wang, Y. H. Lin, O. Cakmakci, and V. Reshetnyak, Phase modulators with tunability in wavefronts and optical axes originating from anisotropic molecular tilts under symmetric electric field II: Experiments, Opt. Express **28** (6), 8985 (2020).
[24] Y. H. Lin, W. C. Cheng, V. Reshetnyak, H. H. Huang, T. W. Huang, C. C. Cheng, Y. H. Wu, and C. L. Yang, Electrically tunable gradient-index lenses via liquid crystals: Beyond the power law, Opt. Express **31** (23), 37843 (2023).
[25] Y. H. Lin, H. Ren, Y. H. Wu, Y. Zhao, J. Fang, Z. Ge, and S. T. Wu, Polarization-independent liquid crystal phase modulator using a thin polymer-separated double-layered structure, Opt. Express **13**, 8746 (2005).
[26] D.-W. Kim, C.-J. Yu, H.-R. Kim, S.-J. Kim, and S.-D. Lee, Polarization-insensitive liquid crystal Fresnel lens of dynamic focusing in an orthogonal binary configuration, Appl. Phys. Lett. **88**, 203505 (2006).
[27] G. Q. Li, P. Valley, P. Ayras, D. L. Mathine, S. Honkanen, and N. Peyghambarian, High-efficiency switchable flat diffractive ophthalmic lens with three-layer electrode pattern and two-layer via structures, Appl. Phys. Lett. **90** (11), 111105 (2007).
[28] J. Bailey, P. B. Morgan, H. F. Gleeson, and J. C. Jones, Switchable liquid crystal contact lenses for the correction of presbyopia, Crystals **8** (1), 29 (2018).
[29] Y. H. Lin, Y. J. Wang, G. L. Hu, and V. Reshetnyak, Electrically tunable polarization independent liquid crystal lenses based on orthogonally anisotropic orientations on adjacent micro-domains, Opt. Express **29**, 29215 (2021).
[30] D. Atchison and G. Smith, *Optics of the Human Eye* (Butterworth-Heinemann, Oxford, 2000).
[31] E. Hecht, *Optics*, 4th ed. (Pearson Education, Upper Saddle River, NJ, 1974).
[32] A. Yariv and P. Yeh, *Optical Waves in Crystals: Propagation and Control of Laser Radiation* (Wiley, New York, 2002).
[33] D. K. Yang and S. T. Wu, *Fundamentals of Liquid Crystal Devices* (Wiley, Chichester, 2006).
[34] A singularity of lens power appearing near the center of the LC optical element within $r = \pm 0.5$ mm is usually ignored in optometry.
[35] S. Wagner, F. Conrad, R. C. Bakaraju, C. Fedtke, K. Ehrmann, and B. A. Holden, Power profiles of single vision and multifocal soft contact lenses, Cont. Lens Anterior Eye **38** (1), 2 (2015).
[36] P. Valley, N. Savidis, J. Schwiegerling, M. R. Dodge, G. Peyman, and N. Peyghambarian, Adjustable hybrid diffractive/refractive achromatic lens, Opt. Express **19** (8), 7468 (2011).
[37] Corresponding video files: https://drive.google.com/drive/folders/1pUl651QfGkSP6sRJZlAPpNSUB3LaCLGo?usp=sharing.
[38] D. W. Berreman, Variable focus liquid crystal lens system. U.S. Patent No. 4,190,330, 26 February 1980.
[39] . B. C. Kress, *Digital Optical Elements and Technologies (EDO19): Applications to AR/VR/MR, B*. edited by C. Kress and P. Schelkens (Proc. SPIE, Germany, 2019), Vol. 11062.
[40] C. Chang, K. Bang, G. Wetzstein, B. Lee, and L. Gao, Toward the next-generation VR/AR optics: a review of holographic near-eye displays from a human-centric perspective, Optica **7** (11), 1563 (2020).
[41] L. Bégel, B. Khodadad, and T. Galstian, Adaptive lens for foveal vision, imaging, and projection over large clear apertures, Opt. Express **31** (2), 2877 (2023).
[42] Some of the data that support the findings of this article are openly available [37]. Others cannot be made publicly available because they contain commercially sensitive information. The data are available upon reasonable request from the authors.